Biochemical and Biophysical Research Communications 632 (2022) 62–68

Contents lists available at ScienceDirect

Biochemical and Biophysical Research Communications

journal homepage: www.elsevier.com/locate/ybbrc

Accelerated aging phenotypes in the retinal pigment epithelium of *Zmpste24*-deficient mice

Jae-Byoung Chae [a, 1], Chul-Woo Park [a, 1], Hyeong Min Lee [b], Leo Sungwong Choi [b], Chaehee Park [a], Junghoon Kim [a], Jaejin Shin [b], Jooseung Hyeon [c], Jihan Lee [c], Hyungwoo Lee [a, d], Hyung Soon Park [b], Chang-Hoon Nam [c], Hyewon Chung [a, d, *]

[a] Department of Ophthalmology, Konkuk University School of Medicine, 120, Neungdong-ro, Gwangjin-gu, Seoul, 05029, South Korea
[b] Glaceum Inc., 3-906, Sinwon-ro, Yeongtong-gu, Suwon, Gyeonggi-do, 16675, South Korea
[c] Aging and Immunity Lab, New Biology Department, Daegu Gyeongbuk Institute of Science and Technology, 333, Techno Jungang-daero, Hyeonpung-myeon, Dalseong-gun, Daegu, 42988, South Korea
[d] Department of Ophthalmology, Konkuk University Medical Center, 120-1, Neungdong-ro, Gwangjin-gu, Seoul, 05029, South Korea

ARTICLE INFO

Article history:
Received 9 September 2022
Received in revised form
12 September 2022
Accepted 15 September 2022
Available online 25 September 2022

Keywords:
Zmpste24
AMD
Senescence
RPE
Retina

ABSTRACT

Age-related macular degeneration (AMD) is a chronic and progressive disease characterized by degeneration of the retinal pigment epithelium (RPE) and retina that ultimately leads to loss of vision. The pathological mechanisms of AMD are not fully known. Cellular senescence, which is a state of cell cycle arrest induced by DNA-damage or aging, is hypothesized to critically affect the pathogenesis of AMD. In this study, we examined the relationship between cellular senescence and RPE/retinal degeneration in mouse models of natural aging and accelerated aging. We performed a bulk RNA sequencing of the RPE cells from adult (8 months old) and naturally-aged old (24 months old) mice and found that common signatures of senescence and AMD pathology – inflammation, apoptosis, and blood vessel formation – are upregulated in the RPE of old mice. Next, we investigated markers of senescence and the degree of RPE/retinal degeneration in *Zmpste24*-deficient (*Zmpste24*$^{-/-}$) mice, which is a model for progeria and accelerated aging. We found that *Zmpste24*$^{-/-}$ mice display markedly greater level of senescence-related markers in RPE and significant RPE/retinal degeneration compared to wild-type mice, in a manner consistent with natural aging. Overall, these results provide support for the association between cellular senescence of RPE and the pathogenesis of AMD, and suggest the use of *Zmpste24*$^{-/-}$ mice as a novel senescent RPE model of AMD.

1. Introduction

Cellular senescence is a state of permanent cell cycle arrest in aged or genomic-damaged cells. Senescence is induced by a variety of stresses, such as mitochondrial dysfunction, severe DNA damage, inflammatory stress, and oxidative stress [1]. Senescence is stimulated by the induction of the tumor suppressor p53 or the cyclin-dependent kinase 2 (CDK2) inhibitor p21. Activation of the p53 pathway causes cell growth arrest, principally via upregulation of the expression of the cell cycle inhibitor p21 and the induction of G1 phase cycle arrest [2]. Senescent cells acquire a senescence-associated secretory phenotype (SASP) and generate a variety of related factors, including cytokines, chemokines, and matrix metalloproteinases. SASP proteins accelerate the cellular senescence process of nearby cells and mediate multiple organismal effects including immune evasion, tumor promotion, and mitochondrial dysfunction within the affected tissue [3,4].

Cellular senescence of the retinal pigment epithelium (RPE) is thought to play a key role in the pathology of age-related macular degeneration (AMD) [5]. AMD is a multifactorial chronic disease and a major cause of irreversible blindness in elderly individuals worldwide [6,7]. AMD is characterized by continuous degeneration of the RPE, Bruch's membrane, choriocapillaris, and retina. The RPE layer is composed of a single polarized layer of hexagonal cells. RPE

* Corresponding author. Department of Ophthalmology, Konkuk University School of Medicine, Konkuk University Medical Center, 120-1 Neungdong-ro, Gwangjin-gu, Seoul, 05030, South Korea.
E-mail address: hchung@kuh.ac.kr (H. Chung).
[1] These two authors contributed equally to this work.

https://doi.org/10.1016/j.bbrc.2022.09.061
0006-291X/

cells carry out many important functions, including ion and fluid transport, phagocytosis of photoreceptor outer segments, and polarized secretion of multiple factors [8,9]. The potential association between the cellular senescence of the RPE and the retinal degeneration in AMD was recently investigated and corroborated by our recent studies where we found that targeted elimination of senescent cells ameliorates retinal degeneration in AMD mouse models [10,11]. Also, the pathological mechanisms of the chemical-induced senescent RPE mouse model were investigated using techniques such as single-cell RNA sequencing of the RPE cells [10,12]. However, the exact mechanisms of and the relationship between retinal degeneration and RPE senescence are not fully known, and there is a need for additional animal models that can represent aging and age-associated changes in the RPE.

Progeria, also known as the Hutchinson-Gilford progeria syndrome (HGPS), is caused by a de novo point mutation in the lamin A/C gene (LMNA) and is characterized by accelerated aging. Patients with progeria exhibit multiple premature aging symptoms, including growth failure, hair loss, bone weakness, and early mortality [13]. The pathological effects of progeria have been well studied in heart, muscle, kidney, bone, and liver tissues of humans and mice. However, in the ocular systems, only the loss of eyebrows and eyelashes and lagophthalmos have been reported [14], and the pathological changes that occur in the RPE or retina are unknown [15,16].

As a mouse model of progeria and accelerated aging, zinc metallopeptidase STE24 homolog (*Zmpste24*) knockout mice are commonly used. *Zmpste24* is a metalloproteinase responsible for cleaving the carboxylic group of prelamin A for the development of mature lamin A [17–19]. *LMNA* is a vital component of the nuclear lamina, which plays roles in nuclear membrane structure, nuclear pore positioning, gene expression, DNA replication, and multiple types of chromatin organization [20]. Both *Zmpste24*- and *LMNA*-deficient mice demonstrate severe nuclear abnormalities and various age-related pathological defects that phenocopy an accelerated senescence process [17,21]. *Zmpste24*$^{-/-}$ mice exhibit accelerated aging resulting in weight loss, spontaneous bone fracture, cardiomyopathy, and muscular dysfunction [21,22]. Additionally, *Zmpste24* deficiency leads to upregulation of senescence-related p53 target genes, resulting in the expression of progeria-like phenotypes in the kidneys, liver, and heart [23].

In this study, we comprehensively analyzed the gene expression of naturally aged adult and old mouse RPE cells by using bulk RNA sequencing (bulk RNA-seq) and found signatures consistent with cellular senescence in the RPE cells of old mice. We investigated the RPE and retina in *Zmpste24*$^{-/-}$ mice as a model of accelerated aging and characterized for the first time the age-related target genes and phenotypes in the RPE and retinal cells of the *Zmpste24*$^{-/-}$ mice. Our findings support the hypothesis that cellular senescence is closely linked to the pathogenesis of AMD and the potential use of *Zmpste24*$^{-/-}$ mice as a model of senescence-induced AMD.

2. Methods

2.1. Experimental animals (*Zmpste24*$^{-/-}$ mice)

The animal care and experimental procedures using mice were approved by the Institutional Animal Care and Use Committee (IACUC) at Daegu Gyeongbuk Institute of Science and Technology (DGIST-IACUC-21112504-0001) and were in accordance with the National Institute of Health Guide for the Care and Use of Laboratory Animals. *Zmpste24*$^{-/-}$ mice were generated and genotyped as previously described [17]. Briefly, *Zmpste24* heterogeneous mice (+/−) were provided by Dr. Zhongjun Zhou (Li Ka Shing Faculty of Medicine, University of Hong Kong) [17]. *Zmpste24*$^{-/-}$ mice were obtained by mating *Zmpste24* heterogenous mice (+/−). The *Zmpste24*$^{-/-}$ mice were genotyped by PCR to confirm the *Zmpste24* allele. All mice were housed in microisolator cages under specific pathogen-free conditions and maintained in a 12:12 h dark/light cycle in a humidity and temperature control facility with ad libitum access to food and water.

2.2. Western blot analysis

Mouse retinal or RPE tissues were lysed in RIPA lysis buffer (Pierce, 89901, Rockford, IL, USA) containing a protease inhibitor cocktail (Roche, 11697498001, Basel, Switzerland). A BCA assay (Pierce, 23227) was performed to quantify the protein concentration according to manufacturer's instructions. Equal amounts of protein samples were loaded and separated by SDS–PAGE and the proteins in the gels were transferred to polyvinylidene difluoride (PVDF) membranes. To block non-specific binding, the PVDF membranes were incubated with 5% nonfat dry milk in Tris buffer containing 0.05% Tween-20 (TBS-T) for 1 h, followed by overnight incubation at 4 °C with anti-p53 (1:500, Santa Cruz Biotechnology, SC-126, Dallas, TX, USA), anti-p21 (1:500, Santa Cruz Biotechnology, SC-6246), anti-p16 (1:1000, Abcam, ab189034, Cambridge, UK), anti-lamin A/C (1:1000, Santa Cruz Biotechnology, SC-376248), and anti-β-actin (1:2000, Santa Cruz Biotechnology, SC-47778) antibodies. Finally, the blots were incubated with horseradish peroxidase (HRP)-conjugated anti-mouse IgG (1:5000, Cell Signaling Technology, 7076S, Boston, MA, USA) or HRP-conjugated anti-rabbit IgG (1:5000, Cell Signaling Technology, 7074S) antibodies in 5% nonfat dry milk TBS-T buffer for 2 h. The immunoreactive proteins were visualized using Femto chemiluminescence substrate (Pierce, 34095). All experiments were performed at least three times.

2.3. RNA isolation and real-time PCR

Total RNA was extracted from harvested mouse retinal or RPE tissues using TRIzol reagent (Invitrogen, 15596026) according to manufacturer's instructions. The mRNA of the isolated RNA was transcribed into cDNA using iScript reverse transcriptase (Bio-Rad Laboratories, #1708890, Hercules, CA, USA). Mouse mRNA expression using specific primers was amplified and quantified with TOPreal™ SYBR Green qPCR PreMIX (Enzynomics, RT500S) using a CFX96 Real-Time PCR detection system (Bio-Rad, CFX96). The levels of relative mRNA expression were analyzed using the $2^{-\Delta\Delta Ct}$ method and the expression levels of GAPDH were used as the internal reference gene. Real-time PCR was performed at least three times for each group. The primers used in this study are shown in Supplementary Table 1.

2.4. Senescence-associated β-galactosidase (SA-β-gal) staining

Sectioned retinal tissues were washed with cold PBS and the fixative solution in the SA-β-gal staining kit (BioVision Inc., K320, Milpitas, CA, USA) was used to fix tissues. Then, the samples were incubated with SA-β-gal staining reagent at 37 °C overnight. All images were captured using an inverted microscope (Olympus, CKX53, Tokyo, Japan).

2.5. Immunofluorescence

Mouse RPE/choroid flat mounts and sectioned retinal tissues were fixed with 4% paraformaldehyde (PFA) for 15 min and permeabilized with 0.1% Triton X-100 in PBS for 10 min at room temperature. After blocking with 1% BSA in PBS for 1 h, the tissues were incubated overnight at 4 °C with anti-p53 (1:100); anti-p21

(1:100); anti-ZO-1 (1:1000, Invitrogen, 61-7300); anti-Nrf2 (1:100, Santa Cruz Biotechnology, SC-365949); anti-NQO1 (1:50, Santa Cruz Biotechnology, SC-32793); anti-heme oxygenase 1 (1:50, Santa Cruz Biotechnology, SC-136960); anti-opsin, blue (1:500, Millipore, AB5407, Billerica, MA, USA); anti-opsin, red/green (1:1000, Millipore, AB5405); and anti-rhodopsin (1:1000, Millipore, MAB5356) antibodies. After overnight incubation, the samples were washed with PBS and incubated for 2 h at room temperature with Alexa Fluor 488- or 555-conjugated secondary antibodies (1:2500, A-11029, A-21424, A-21427, A-11034, Thermo Fisher Scientific, A-Waltham, MA, USA). The nuclei were counterstained with Hoechst 33342 (1:1000, Thermo Fisher Scientific, H3570) in PBS for 15 min at room temperature. The stained samples were mounted with Aqua Poly/Mount mounting medium (Polysciences, Inc., 18606-20, Warrington, PA, USA) and visualized with an inverted microscope (Carl Zeiss A.G., LSM900, Oberkochen, Germany).

2.6. Cryosectioning and histology

Mouse eyes were enucleated, trimmed, and eye cups were isolated, followed by fixation in 4% PFA for 6 h at 4 °C. The fixed eye cups were transferred to 15% sucrose in PBS for 6 h at 4 °C and transferred to 30% sucrose in PBS for at least 2 h until the eye cups settled to the bottom. The sucrose equilibrated eye cups were embedded in O.C.T compound (Leica Biosystems Inc., 3801480, Wetzlar, Germany) with cryomolds and stored in −80 °C. The frozen blocks were sectioned with a cryostat (Leica Biosystems Inc., Leica CM1860) at 10-μm thickness and serial frozen sections were stained with hematoxylin and eosin (H&E) staining. The thickness of outer nuclear layer (ONL) and inner nuclear layer (INL) of the retina was measured by the stained samples using ImageJ software (NIH, USA). The averages of thickness ONL, INL, and whole retina thickness were measured at least three different sections.

2.7. TUNEL assay

For the detection of apoptosis in retina tissues, the In Situ Cell Death Detection Kit (Roche, 11684795910) was used according to manufacturer's instructions with slight modifications. Briefly, sectioned retina slides were fixed with 4% PFA for 15 min and washed with PBS. The tissues were incubated with 50 μL of TUNEL reaction mixture for 1 h at 37 °C in a humidified atmosphere in the dark. The nuclei were counterstained with Hoechst 33342 (1:1000, Thermo Fisher Scientific), and the stained tissue was observed with an inverted microscope (Carl Zeiss A.G., LSM900).

2.8. Bulk RNA-seq analysis

The concentration of total RNA was measured with Quant-IT RiboGreen (Invitrogen, R11490). To confirm the quality of the extracted total RNA, the RNAs were loaded and run on a TapeStation RNA ScreenTape device (Agilent Technologies, 5067-5576, Santa Clara, CA, USA). The high-quality RNA with RNA integrity numbers (RINs) more than 7.0 were processed for RNA library construction. Each library was independently prepared with 0.5 μg of total RNA for each sample with an Illumina TruSeq Stranded Total RNA Library Prep Gold Kit (Illumina, Inc., 20020599, San Diego, CA, USA). First, the rRNA from the total RNA was removed, and then the residual mRNA was cleaved into small portions with divalent cations at elevated temperature. The fragmented RNA portions were reverse transcribed into cDNA by SuperScript II reverse transcriptase (Invitrogen, 18064014) with random hexamers. The synthesized first-strand cDNA was used as a template for generating second-strand cDNA using DNA Polymerase I, RNase H and dUTP. The synthesized cDNA fragments were prepared with an end repair process, a single 'A' base addition, and adapter ligation. The DNA products were refined and amplified with PCR to generate the cDNA library. The prepared libraries were quantified with KAPA Library Quantification kits with Illumina Sequencing Platforms according to the qPCR Quantification Protocol Guide (KAPA BIOSYSTEMS, KK4854, Potters Bar, United Kingdom) and qualified with the TapeStation D1000 ScreenTape device (Agilent Technologies, 5067-5582). The indexed libraries were then subjected paired-end (2 × 100 bp) sequencing on an Illumina NovaSeq (Illumina, Inc.). The raw reads from the sequencer were preprocessed to remove low-quality and adapter sequences prior to analysis and aligned the processed reads to the *Mus musculus* genome (GRCm38) using Bowtie2 v2.3.4.1 [24]. The reference genome sequence and annotation data were downloaded from Ensembl. Then, the known transcripts were assembled with featureCounts v1.6.0 [25]. Based on the results, the expression abundance of transcripts and genes was calculated as the read counts or values (fragments per kilobase of exon per million fragments mapped, FPKM) per sample. To explore the signaling pathways in which the differentially expressed genes (DEGs) were enriched, Gene Ontology (GO) enrichment and Kyoto Encyclopedia of Genes and Genomes (KEGG) pathway analyses were performed using g:Profiler. To construct a network depicting the enriched processes, GO-BP-based network analysis was visualized and interpreted in Cytoscape using Enrichment Map.

2.9. Statistics

All experimental data are presented as the mean ± SD. Statistical significance (the *P* value) was determined using unpaired two-tailed Student's *t* tests followed by Fisher's least significant difference post hoc test or Tukey's multiple comparisons test. Data were analyzed using GraphPad Prism software (San Diego, CA, USA). Statistical significance was defined as $p < 0.05$ (* $p < 0.05$, ** $p < 0.01$, *** $p < 0.001$).

3. Results and discussion

3.1. Analysis of differentially expressed genes in old mouse RPE cells

We first examined the effects of natural aging on the RPE cells of wild-type mice. The differential gene expression in the RPE cells of three adult (8 months old) and three old (24 months old) mice was analyzed by bulk RNA-seq. The resultant gene expression is shown in the volcano plot (Fig. 1A), where significantly ($P < 0.05$) differentially expressed genes (DEGs) of the old mice RPE compared to the adult mice RPE were identified. There was a greater number of upregulated DEGs compared to downregulated DEGs, and we focused further analysis on these upregulated DEGs to find potential markers of RPE senescence. To detect which biological pathways are influenced by aging, Gene Ontology (GO) analysis focusing on the biological process (BP) and Kyoto Encyclopedia of Genes and Genomes (KEGG) analysis were performed. Interestingly, the most upregulated BP terms included signal transduction, immune response, apoptotic process, and blood vessel development (Fig. 1B). The upregulated immune response is in line with the reported increase of inflammatory environment induced by cellular senescence and the SASP of senescent cells, which eventually leads to signals of apoptosis. Also, the upregulated blood vessel development is highly relevant to the precipitation of choroidal neovascularization in AMD. These upregulated pathways in the GO-BP analysis suggest that senescence is related to increased inflammation signaling, altered signal transduction, apoptosis, and neovascularization in RPE. In KEGG analysis, the top upregulated

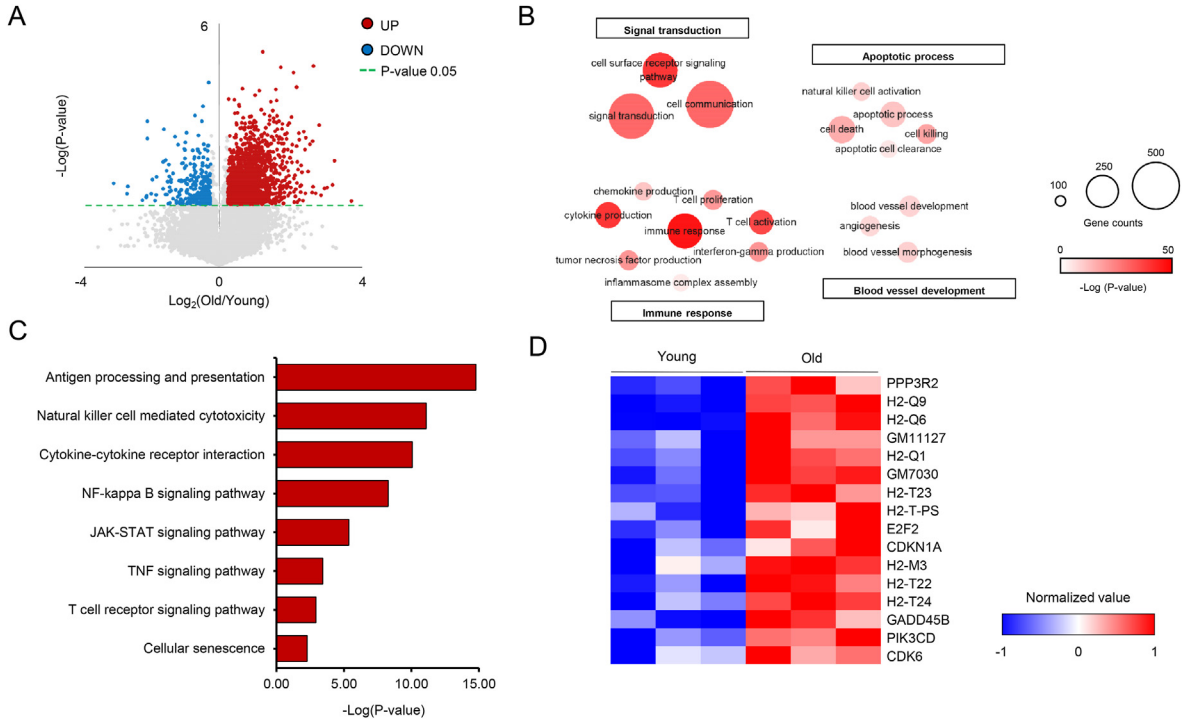

Fig. 1. Differentially expressed genes (DEGs) in the retinal pigment epithelium (RPE) cells isolated from old mice in comparison to those from adult mice. Bulk-RNA seq analysis was performed on the RPE isolated from the old mice (24 months old; n = 3) and the adult mice (8 months old; n = 3).
(A) Volcano plot of DEGs of the old mice RPE cells in comparison to the adult mice RPE cells. Genes upregulated or downregulated by more than 1.2-fold with P-value < 0.05 are shown in red and blue, respectively. The upregulated genes were selected for further analysis. (B) Network modeling of the most significant Gene Ontology (GO) biological processes of the upregulated genes. The legends for color coding and gene counting are shown on the right. (C) KEGG pathway analysis of the upregulated genes, showing the most significantly altered pathways in a ranked order. (D) Heatmap of the individual upregulated DEGs that are associated with cellular senescence. .

signaling pathways were all related to inflammation, including the NF-kappa B, JAK-STAT, and TNF signaling pathways (Fig. 1C). Notably, cellular senescence was also detected among the top upregulated KEGG pathways, suggesting that cellular senescence is indeed upregulated in the RPE cells of old mice. To specifically determine which genes in the cellular senescence pathway are upregulated to what degree, the name and expression of all 16 genes from each animal were depicted as a heatmap (Fig. 1D). Of note, among these genes, CDKN1A encodes the p21 protein, wherein its increase plays a pivotal role in cellular senescence. Overall, the transcriptomic analysis data demonstrate that cellular senescence and signatures of AMD – inflammation, apoptosis, and neovascularization – are upregulated in the RPE of naturally aged old mice.

3.2. Deficiency of Zmpste24 accelerates senescence in the mouse RPE

To evaluate the cellular senescence features in the RPEs and retinas of *Zmpste24*$^{-/-}$ mice, we compared the SA-β-gal activity as a biomarker of cellular senescence in 12-week-old *Zmpste24*$^{-/-}$ mice with those of their wild-type littermates. Markedly increased SA-β-gal activity in the RPE and retina was observed in *Zmpste24*$^{-/-}$ mice compared to wild-type mice (Fig. 2A). Next, we investigated the expression of the major senescence markers p53 and p21; *Zmpste24* deficiency is reported to promote p53 signaling activation and upregulate p53-related target genes [23]. In the RPE layer, the expression of both p53 and p21 was remarkably higher in *Zmpste24*$^{-/-}$ mice than that in wild-type mice (Fig. 2B and C). Consistent with these findings, Western blot analysis showed higher p53, p21, and p16 levels in RPE cells from *Zmpste24*$^{-/-}$ mice than in those from wild-type mice (Fig. 2D). *Zmpste24*$^{-/-}$ mice are defective in proteolytic processing of prelamin A [26], and accumulation of prelamin A leads to abnormalities in nuclear envelopes and to loss of mature lamin A [17,18,23]. As expected, Western blot analysis of lamin A/C showed significantly lower levels of lamin A in the RPE in *Zmpste24*$^{-/-}$ mice than in wild-type mice (Fig. 2D). The mRNA expression of the senescence markers p53 and p21 and the SASP factors vascular endothelial growth factor A (VEGFA), interleukin 1α (IL-1α), interleukin 1β (IL-1β), and interleukin 6 (IL-6) was also increased significantly in the RPE tissues from *Zmpste24*$^{-/-}$ mice compared to those from wild-type mice (Fig. 2E). In retina, however, neither the protein nor the mRNA expression of p53, p21 and SASP factors except for IL-6 was significantly increased in *Zmpste24*$^{-/-}$ mice compared to wild-type mice (Fig. 2B, D, and 2E). Collectively, these results show that cellular senescence is robustly observed in the posterior eyeball segments of *Zmpste24*$^{-/-}$ mice, mainly in the RPE layer.

3.3. Deficiency of Zmpste24 induces retinal degeneration

We investigated whether accelerated senescence of the RPE in *Zmpste24*$^{-/-}$ mice indeed contributes to the retinal degeneration. H&E staining of cryosectioned retinas showed that both the INL and ONL are thinner in *Zmpste24*$^{-/-}$ mice than in wild-type mice, and significant reduction of retinal thickness is observed in *Zmpste24*$^{-/-}$ mice (Fig. 3A). There was also increased numbers of TUNEL-positive cells in the retinas from *Zmpste24*$^{-/-}$ mice (Fig. 3B), which suggest that the retinal thickness may have been reduced due to apoptotic cell death of retinal cells.

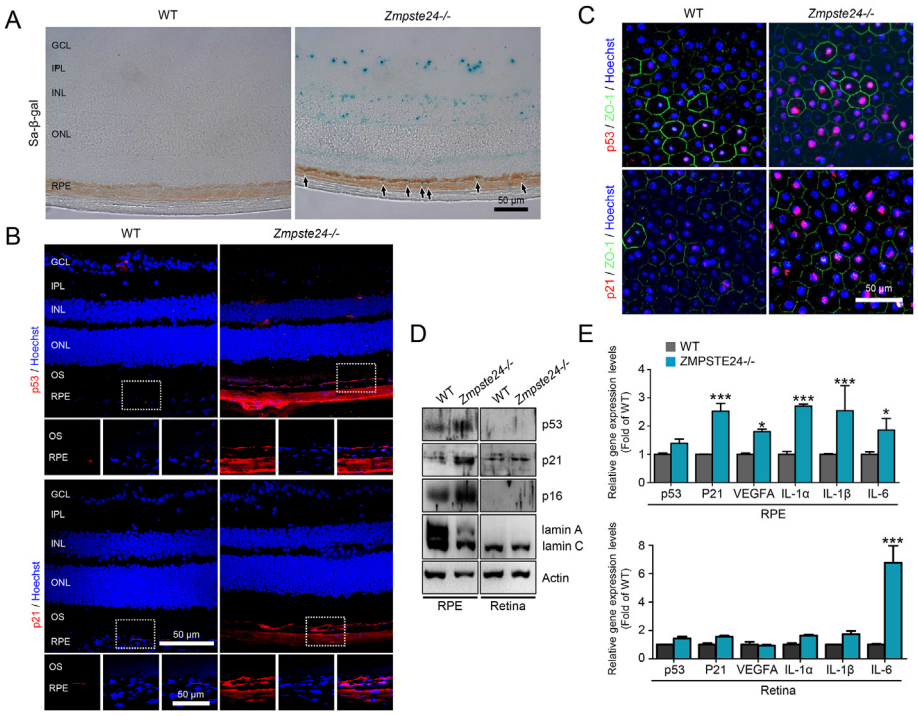

Fig. 2. Accelerated senescence phenotypes in the *Zmpste24*$^{-/-}$ mouse RPE.
(A) SA-β-galactosidase (SA-β-gal) staining in cryosectioned retinas. SA-β-gal-positive areas in the RPE layer are outlined by black arrowheads. (B) Immunofluorescence staining of p53 and p21 in cryosectioned retinas. The insets depict the layers, including photoreceptor inner and outer segments (IS/OS) and RPE. (C) Immunofluorescence staining of p53, p21, and ZO-1 in RPE flat mounts. Nuclei were stained with Hoechst. (D) Western blot analysis of senescence markers and lamin A/C in the RPE and retina. (E) mRNA expression of senescence markers and SASP factors by real-time PCR. GCL, ganglion cell layer; IPL, inner plexiform layer; INL, inner nuclear layer; ONL, outer nuclear layer; IS/OS, photoreceptor inner and outer segments; RPE, retinal pigment epithelium. The data are presented as the mean ± SD. *$P < 0.05$, ** $P < 0.01$, and ***$P < 0.001$ by *t*-test. The scale bars in (A–C) represent 50 μm.

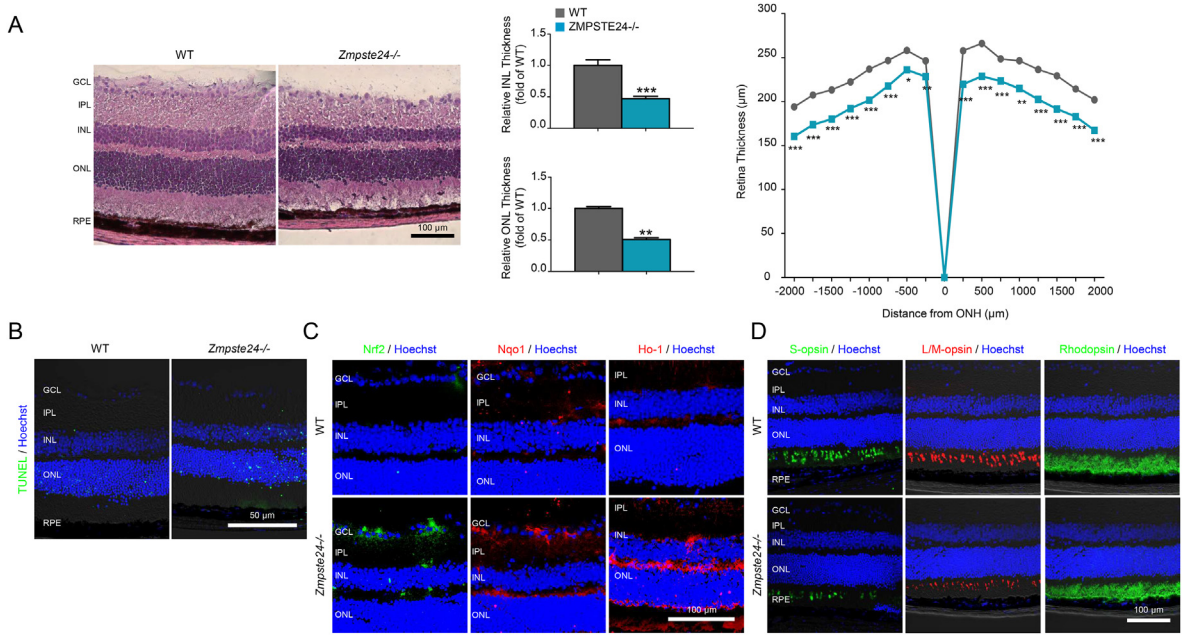

Fig. 3. A senescent RPE facilitates retinal degeneration in *Zmpste24*$^{-/-}$ mice
(A) Hematoxylin and eosin (H&E)-stained images of retinal sections (left). Quantification of the inner nuclear layer (INL) thickness and outer nuclear layer (ONL) thickness (middle). When *Zmpste24*$^{-/-}$ mice were compared with wild-type mice, the INL and the ONL thickness was decreased by approximately 2.12- and 1.97-fold, respectively. Whole retinal thickness measured on sections at 250 μm intervals starting at the optic nerve head (ONH) (right). (B) Immunofluorescence labeling of cryosectioned retinas with a TUNEL labeling kit. (C) Immunofluorescence staining of Nrf2 (left), Nqo1 (middle), and Ho-1 (right) in cryosectioned retinas. (D) Immunofluorescence staining of S-opsin (left), L/M-opsin (middle), and rhodopsin (right) in cryosectioned retinas. GCL, ganglion cell layer; IPL, inner plexiform layer; INL, inner nuclear layer; ONL, outer nuclear layer; IS/OS, photoreceptor inner and outer segments; RPE, retinal pigment epithelium. The data are presented as the mean ± SD. *$P < 0.05$, ** $P < 0.01$, and ***$P < 0.001$ by *t*-test. The scale bars in (A–D) represent 100 μm.

In addition to the evident retinal degeneration observed, the antioxidative and anti-inflammatory capacity of the RPE from *Zmpste24*$^{-/-}$ mice was investigated. This was because inflammation is a key aspect of both senescence and AMD and inflammation was specifically increased in the RPE of old mice. The expression levels of nuclear factor erythroid-2-related factor 2 (Nrf2) and its downstream targets NAD(P)H quinone dehydrogenase 1 (Nqo1) and heme oxygenase 1 (Ho-1) were examined in the cryosectioned retinas, because the Nrf2 signaling pathway is a key regulator of inflammation [27–29]. Nrf2 expression was increased prominently in the retinal ganglion cell layer in *Zmpste24*$^{-/-}$ mice; the expression of Nqo1 and Ho-1 was also markedly increased in most retinal layers in *Zmpste24*$^{-/-}$ mice compared to wild-type mice (Fig. 3C). The significantly increased expression levels of Nrf2, Nqo-1, and Ho-1 in the retinas in *Zmpste24*$^{-/-}$ mice suggest that inflammatory stress indeed exists heavily in the retinas of these mice [30–33].

Lastly, to fully evaluate the retinal health, the expression of photoreceptor markers was examined. The levels of expression of the cone photoreceptor markers S-opsin and L/M-opsin and the rod photoreceptor marker rhodopsin were significantly lower in *Zmpste24*$^{-/-}$ mice than in wild-type mice (Fig. 3D), consistent with previous reports of changes in photoreceptors in aged mice and rats [34,35]. Taken together, the overall results indicate that along with the cellular senescence observed, there is significant retinal degeneration in *Zmpste24*$^{-/-}$ mice.

4. Conclusions

In this study, 12-week-old *Zmpste24*$^{-/-}$ mice exhibited cellular senescence of the RPE that was consistent with the transcriptomic patterns of naturally aged mice; also, subsequent degeneration of the retina and RPE was strongly observed. Given the difficulty of maintaining and performing experiments with naturally aged mice over 24 months old, *Zmpste24*$^{-/-}$ mice may be used as a new RPE senescence animal model for potential therapeutics of AMD.

Declaration of competing interest

The authors declare that they have no conflict of interest.

Acknowledgment

This work was supported by a Konkuk University Medical Center Research Grant 2021 (K210119).

Appendix A. Supplementary data

Supplementary data to this article can be found online at https://doi.org/10.1016/j.bbrc.2022.09.061.

References

[1] M. Collado, M.A. Blasco, M. Serrano, Cellular senescence in cancer and aging, Cell 130 (2007) 223–233, https://doi.org/10.1016/j.cell.2007.07.003.
[2] T. Van Nguyen, N. Puebla-Osorio, H. Pang, M.E. Dujka, C. Zhu, DNA damage-induced cellular senescence is sufficient to suppress tumorigenesis: a mouse model, J. Exp. Med. 204 (2007) 1453–1461, https://doi.org/10.1084/jem.20062453.
[3] N. Herranz, J. Gil, Mechanisms and functions of cellular senescence, J. Clin. Invest. 128 (2018) 1238–1246, https://doi.org/10.1172/JCI95148.
[4] J. Campisi, J.K. Andersen, P. Kapahi, S. Melov, Cellular senescence: a link between cancer and age-related degenerative disease? Semin. Cancer Biol. 21 (2011) 354–359, https://doi.org/10.1016/j.semcancer.2011.09.001.
[5] M.R. Kozlowski, RPE cell senescence: a key contributor to age-related macular degeneration, Med. Hypotheses 78 (2012) 505–510, https://doi.org/10.1016/j.mehy.2012.01.018.
[6] L.S. Lim, P. Mitchell, J.M. Seddon, F.G. Holz, T.Y. Wong, Age-related macular degeneration, Lancet 379 (2012) 1728–1738, https://doi.org/10.1016/S0140-6736(12)60282-7.
[7] R.D. Jager, W.F. Mieler, J.W. Miller, Age-related macular degeneration, N. Engl. J. Med. 358 (2008) 2606–2617, https://doi.org/10.1056/NEJMra0801537.
[8] S. Yang, J. Zhou, D. Li, Functions and diseases of the retinal pigment epithelium, Front. Pharmacol. 12 (2021), 727870, https://doi.org/10.3389/fphar.2021.727870.
[9] J.R. Sparrow, D. Hicks, C.P. Hamel, The retinal pigment epithelium in health and disease, Curr. Mol. Med. 10 (2010) 802–823, https://doi.org/10.2174/156652410793937813.
[10] J.B. Chae, H. Jang, C. Son, C.W. Park, H. Choi, S. Jin, H.Y. Lee, H. Lee, J.H. Ryu, N. Kim, C. Kim, H. Chung, Targeting senescent retinal pigment epithelial cells facilitates retinal regeneration in mouse models of age-related macular degeneration, Geroscience 43 (2021) 2809–2833, https://doi.org/10.1007/s11357-021-00457-4.
[11] H. Chung, C. Kim, Nutlin-3a for age-related macular degeneration, Aging (Albany NY) 14 (2022) 5614–5616, https://doi.org/10.18632/aging.204187.
[12] H. Lee, H.Y. Lee, J.B. Chae, C.W. Park, C. Kim, J.H. Ryu, J. Jang, N. Kim, H. Chung, Single-cell transcriptome of the mouse retinal pigment epithelium in response to a low-dose of doxorubicin, Commun Biol 5 (2022) 722, https://doi.org/10.1038/s42003-022-03676-3.
[13] A. De Sandre-Giovannoli, R. Bernard, P. Cau, C. Navarro, J. Amiel, I. Boccaccio, S. Lyonnet, C.L. Stewart, A. Munnich, M. Le Merrer, N. Levy, Lamin a truncation in Hutchinson-Gilford progeria, Science 300 (2003) 2055, https://doi.org/10.1126/science.1084125.
[14] S.L. Chandravanshi, A.K. Rawat, P.C. Dwivedi, P. Choudhary, Ocular manifestations in the Hutchinson-Gilford progeria syndrome, Indian J. Ophthalmol. 59 (2011) 509–512, https://doi.org/10.4103/0301-4738.86327.
[15] R. Varga, M. Eriksson, M.R. Erdos, M. Olive, I. Harten, F. Kolodgie, B.C. Capell, J. Cheng, D. Faddah, S. Perkins, H. Avallone, H. San, X. Qu, S. Ganesh, L.B. Gordon, R. Virmani, T.N. Wight, E.G. Nabel, F.S. Collins, Progressive vascular smooth muscle cell defects in a mouse model of Hutchinson-Gilford progeria syndrome, Proc. Natl. Acad. Sci. U. S. A. 103 (2006) 3250–3255, https://doi.org/10.1073/pnas.0600012103.
[16] L.W. Koblan, M.R. Erdos, C. Wilson, W.A. Cabral, J.M. Levy, Z.M. Xiong, U.L. Tavarez, L.M. Davison, Y.G. Gete, X. Mao, G.A. Newby, S.P. Doherty, N. Narisu, Q. Sheng, C. Krilow, C.Y. Lin, L.B. Gordon, K. Cao, F.S. Collins, J.D. Brown, D.R. Liu, In vivo base editing rescues Hutchinson-Gilford progeria syndrome in mice, Nature 589 (2021) 608–614, https://doi.org/10.1038/s41586-020-03086-7.
[17] A.M. Pendas, Z. Zhou, J. Cadinanos, J.M. Freije, J. Wang, K. Hultenby, A. Astudillo, A. Wernerson, F. Rodriguez, K. Tryggvason, C. Lopez-Otin, Defective prelamin A processing and muscular and adipocyte alterations in Zmpste24 metalloproteinase-deficient mice, Nat. Genet. 31 (2002) 94–99, https://doi.org/10.1038/ng871.
[18] L.G. Fong, J.K. Ng, M. Meta, N. Cote, S.H. Yang, C.L. Stewart, T. Sullivan, A. Burghardt, S. Majumdar, K. Reue, M.O. Bergo, S.G. Young, Heterozygosity for Lmna deficiency eliminates the progeria-like phenotypes in Zmpste24-deficient mice, Proc. Natl. Acad. Sci. U. S. A. 101 (2004) 18111–18116, https://doi.org/10.1073/pnas.0408558102.
[19] L.C. Mounkes, S. Kozlov, L. Hernandez, T. Sullivan, C.L. Stewart, A progeroid syndrome in mice is caused by defects in A-type lamins, Nature 423 (2003) 298–301, https://doi.org/10.1038/nature01631.
[20] R.D. Goldman, Y. Gruenbaum, R.D. Moir, D.K. Shumaker, T.P. Spann, Nuclear lamins: building blocks of nuclear architecture, Genes Dev. 16 (2002) 533–547, https://doi.org/10.1101/gad.960502.
[21] M.O. Bergo, B. Gavino, J. Ross, W.K. Schmidt, C. Hong, L.V. Kendall, A. Mohr, M. Meta, H. Genant, Y. Jiang, E.R. Wisner, N. Van Bruggen, R.A. Carano, S. Michaelis, S.M. Griffey, S.G. Young, Zmpste24 deficiency in mice causes spontaneous bone fractures, muscle weakness, and a prelamin A processing defect, Proc. Natl. Acad. Sci. U. S. A. 99 (2002) 13049–13054, https://doi.org/10.1073/pnas.192460799.
[22] G.K. Leung, W.K. Schmidt, M.O. Bergo, B. Gavino, D.H. Wong, A. Tam, M.N. Ashby, S. Michaelis, S.G. Young, Biochemical studies of Zmpste24-deficient mice, J. Biol. Chem. 276 (2001) 29051–29058, https://doi.org/10.1074/jbc.M102908200.
[23] I. Varela, J. Cadinanos, A.M. Pendas, A. Gutierrez-Fernandez, A.R. Folgueras, L.M. Sanchez, Z. Zhou, F.J. Rodriguez, C.L. Stewart, J.A. Vega, K. Tryggvason, J.M. Freije, C. Lopez-Otin, Accelerated ageing in mice deficient in Zmpste24 protease is linked to p53 signalling activation, Nature 437 (2005) 564–568, https://doi.org/10.1038/nature04019.
[24] B. Langmead, S.L. Salzberg, Fast gapped-read alignment with Bowtie 2, Nat. Methods 9 (2012) 357–359, https://doi.org/10.1038/nmeth.1923.
[25] Y. Liao, G.K. Smyth, W. Shi, featureCounts: an efficient general purpose program for assigning sequence reads to genomic features, Bioinformatics 30 (2014) 923–930, https://doi.org/10.1093/bioinformatics/btt656.
[26] A.K. Agarwal, J.P. Fryns, R.J. Auchus, A. Garg, Zinc metalloproteinase, ZMPSTE24, is mutated in mandibuloacral dysplasia, Hum. Mol. Genet. 12 (2003) 1995–2001, https://doi.org/10.1093/hmg/ddg213.
[27] S.M. Ahmed, L. Luo, A. Namani, X.J. Wang, X. Tang, Nrf2 signaling pathway: pivotal roles in inflammation, Biochim. Biophys. Acta, Mol. Basis Dis. 1863 (2017) 585–597, https://doi.org/10.1016/j.bbadis.2016.11.005.
[28] Z. Zhao, Y. Chen, J. Wang, P. Sternberg, M.L. Freeman, H.E. Grossniklaus, J. Cai, Age-related retinopathy in NRF2-deficient mice, PLoS One 6 (2011), e19456, https://doi.org/10.1371/journal.pone.0019456.
[29] Y. Wei, J. Gong, Z. Xu, R.K. Thimmulappa, K.L. Mitchell, D.S. Welsbie, S. Biswal, E.J. Duh, Nrf2 in ischemic neurons promotes retinal vascular regeneration

through regulation of semaphorin 6A, Proc. Natl. Acad. Sci. U. S. A. 112 (2015) E6927–E6936, https://doi.org/10.1073/pnas.1512683112.
[30] S. Arai-Gaun, N. Katai, T. Kikuchi, T. Kurokawa, K. Ohta, N. Yoshimura, Heme oxygenase-1 induced in muller cells plays a protective role in retinal ischemia-reperfusion injury in rats, Invest. Ophthalmol. Vis. Sci. 45 (2004) 4226–4232, https://doi.org/10.1167/iovs.04-0450.
[31] D. Ross, D. Siegel, The diverse functionality of NQO1 and its roles in redox control, Redox Biol. 41 (2021), 101950, https://doi.org/10.1016/j.redox.2021.101950.
[32] N. Himori, K. Yamamoto, K. Maruyama, M. Ryu, K. Taguchi, M. Yamamoto, T. Nakazawa, Critical role of Nrf2 in oxidative stress-induced retinal ganglion cell death, J. Neurochem. 127 (2013) 669–680, https://doi.org/10.1111/jnc.12325.
[33] H.M. Schipper, W. Song, H. Zukor, J.R. Hascalovici, D. Zeligman, Heme oxygenase-1 and neurodegeneration: expanding frontiers of engagement, J. Neurochem. 110 (2009) 469–485, https://doi.org/10.1111/j.1471-4159.2009.06160.x.
[34] A. Cunea, M.B. Powner, G. Jeffery, Death by color: differential cone loss in the aging mouse retina, Neurobiol. Aging 35 (2014) 2584–2591, https://doi.org/10.1016/j.neurobiolaging.2014.05.012.
[35] A. Cunea, G. Jeffery, The ageing photoreceptor, Vis. Neurosci. 24 (2007) 151–155, https://doi.org/10.1017/S0952523807070204.